Computer simulation of polar bent-core molecules

Stephen J. Johnston, Robert J. Low, and Maureen P. Neal*
School of Mathematical and Information Sciences, Coventry University, Coventry, CV1 5FB, United Kingdom
(Received 15 April 2002; published 12 December 2002)

Results are presented from molecular dynamics simulations in the *NPT* ensemble of novel bent-core liquid crystal systems. Following on from a previous study of bent-core steric shape, this study examines the effect the addition of a transverse electric dipole has on the phase diagram of a bent-core liquid crystal model. A simple model of the interaction employed a two-site Gay-Berne potential with the sites separated by ± 0.5 reduced units with a central transverse point dipole, for all models investigated. The angle between the sites $180° - \gamma$ was varied in a range $\gamma = 10°$ to $\gamma = 70°$ suggested by real molecules. The addition of the dipole to the model tended to stabilize smectic phases and increase the angle of tilted phases. As the angle γ increased, the transition temperature to the first ordered phase decreased markedly. Smectic *A*, tilted smectic *B*, and a spontaneously polarized smectic *B* phases were observed in the $\gamma = 10°$ bent-core model. The $\gamma = 20°$ model showed smectic *A* and tilted antiferroelectric smectic *B* phases. The $\gamma = 40°$ model showed an antiferroelectric phase that exhibited unusual packing behavior. Both the $\gamma = 20°$ and $\gamma = 40°$ models demonstrated a significant phase biaxiality in the smectic *B* phases.

DOI: 10.1103/PhysRevE.66.061702 PACS number(s): 61.30.−v, 61.20.Ja

I. INTRODUCTION

Bent-core liquid crystalline systems have ferroelectric properties [1] and form chiral phases despite the constituent molecules being achiral. They have been the focus of a range of experimental, synthetic, and simulation studies because of their unusual properties. Many liquid crystal molecules possess polar groups that may have an influence on the types of phases observed and the point in the phase space where the transition occurs. As such the addition of electrostatic forces to anisotropic models has been the focus of many computer simulations e.g., Refs. [2–4]. Of particular interest here is the effect the addition of a polar group has on the phase behavior of systems of bent-core molecules. The bent-core models, based on the P-*n*-PIMB molecule [1], have a strong dipole moment transverse to the long molecular axis, in the direction of bend of the bent core, of the order of two debyes. Niori *et al.* [1] proposed that polar alignment of molecules constrained to a smectic layer as the structure to explain ferroelectric ordering.

The relative effects of steric and electric contributions [5], to the packing of the molecules has been the subject of several studies, e.g., Refs. [6,7]. Simulations of apolar bent-core molecules, considered a transverse steric dipole, have shown some of the unusual packing features of real bent-core molecules [8–12].

Theoretical studies have concentrated on the ability of these achiral bent-core shapes to form chiral phases. Brand *et al.* [13] showed how a system of bent-core molecules constrained to smectic layers can be chiral. This happens if the bent cores were rotated about their polar axis whilst still constrained to the smectic layer, creating adjacent smectic layers with either synclinic or anticlinic tilt. In such an arrangement, the symmetry of the system is reduced to the point where chirality occurs. This is the arrangement seen in the most prevalent bent-core phase, the $B2$ phase in both ferroelectric [14] and antiferroelectric [15] phases. A full review is found in Pelzl *et al.* [16] and includes descriptions of the phases found to date including the tilted $B2$ phase, hexatic-like $B3$ phase and two-site Gay-Berne ''TGB-like'' $B4$ phase.

Simulation studies to date have been reported for hard and soft models of apolar bent-core systems. Camp *et al.* [8] studied a hard rod system composed of spherocylinders where each molecule was modeled by two spherocylinder subunits joined at their ends giving an overall length-to-breadth ratio of 4:1 for the rodlike model. The displacement of the spherocylinders was then kept constant for all values of the angle of bend studied. For small deviations from the rodlike model, $\gamma = 10°$ and 20°, normal nematic and smectic liquid crystal phases were found. For a larger deviation of 30°, the smectic phase was destabilised with a transition from the nematic phase straight to a biaxial solid. At higher degrees of bend, the molecules were found to form interlocking pairs suppressing the formation of any liquid crystal phases. In a second study [9] the bent-core shape was modeled using a two-site Gay-Berne [17] potential with the sites displaced to the extremes of the zero potential surface producing a model very much like Ref. [8], but with an overall length-to-breadth ratio of 6:1 for the rod-like model. The angle between the ''wings'' of the bent-core was fixed at 140° i.e., $\gamma = 40°$, with the simulations conducted in the isothermal-isobaric ensemble (NPT). Similarly to the hard rod model an isotropic-smectic phase transition was identified and evidence of a chiral superstructure was found, although its presence has yet to be confirmed. As the temperature was decreased a nematic-smectic phase transition was identified with no interdigitation and a local phase biaxiality and polarization. The layer arrangement was that of an antiparallel structure. While the model was an apolar electric system it was termed as a transverse steric ''polar'' system [5]. Both of these models have shown classical liquid crystal

*Corresponding author;
Email address: m.p.neal@coventry.ac.uk

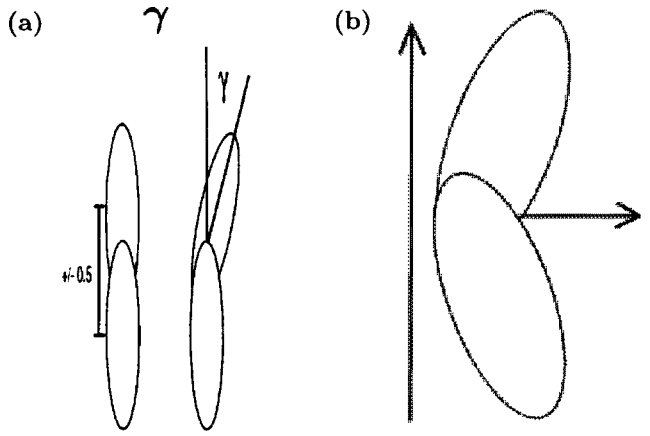

FIG. 1. Schematic representation of (a) a two-site bent-core molecule and (b) the addition of a dipole to the polar bent-core molecule.

phases rather than the more unusual phases that the bent-core molecules display. A recent report by Xu *et al.* [10] used a multisite Lennard-Jones-type model arranged such that the bend in the molecule was the same as that in Ref. [9]; an angle of $\gamma=40°$. They also found chiral symmetry-breaking behavior with the molecules tilting with respect to the layer normal in the crystalline phase, however, the direction of the tilt was not aligned or alternating from layer to layer unlike the packing seen in the real molecules. Upon heating the tilt disappeared and there was a phase transition to the smectic *A* phase. The simulation was undertaken in the *NVT* ensemble which may affect the packing density. While the total volume was kept fixed, the aspect ratio was allowed to fluctuate. Maiti *et al.* [11] examined a hard rod mixture of bent-core and rodlike molecules. The rodlike molecules were modeled with a spherocylinder, length-to-breadth ratio of 5:1 and the bent-core molecules had an overall length-to-breadth ratio of either 5:1 or 10:1. They found that in the smectic phase, the presence of a small quantity of length-to-breadth ratio 10:1 bent-core molecules caused an anticlinic tilt to develop providing γ was less than 80°. For values of $\gamma>80°$ the bent-core molecules arranged themselves between the smectic layers and no tilt was observed. No tilt was observed in the mixture of rodlike molecules and length-to-breadth ratio 5:1 bent-core molecules. No evidence of the *B*2 phase or any steric polar ordering has been reported to date. It is therefore of considerable interest to observe the effect of a transverse dipole on the phase diagram of a bent-core model.

The study presented in this paper will investigate the effect of the addition of a transverse electric dipole to the transverse steric dipole shape. A previous study [12] was undertaken by the authors of a two-site bent-core molecule shown in Fig. 1(a), modeled by two Gay-Berne [17] sites at varying angles of γ. For a rodlike model normal nematic, smectic *A* and smectic *B* phases were observed. As the value of γ was increased, the nematic phase was initially destabilised with a transition directly to a smectic *A* phase. As γ was increased further the nematic phase was stabilised and tilted smectic phases were observed. For a value of $\gamma=40°$, a biaxial ''TGB-like'' phase was found but no in-layer tilt was observed. No steric polar ordering was observed for any of the models studied. The addition of the electric dipole to this model, the details of which are explained later, has the effect of adding additional realism to the model and this study was undertaken to determine whether the effect of this addition leads to the development of polar order in the system.

The authors have previously reported [18] the effect of the addition of a transverse dipole on the rodlike molecule. Compared with the apolar rodlike molecule the nematic phase was destabilised with a transition directly to a smectic *B* phase then to a ferroelectric crystal. Several other studies involving transverse dipoles have been conducted for the standard rodlike models. Houssa *et al.* [19] examined a model composed of a Gay-Berne site with a transverse dipole moment of varying strength. They found that for a significantly strong dipole moment the normal phase transition of isotropic to nematic to smectic *B* was disrupted, and a transition straight to the smectic *B* phase was observed. Gil-Villegas *et al.* [20] undertook a study of a system of hard rods with transverse point dipoles. The dipolar potential was seen to stabilize the smectic *A* phase with respect to the nematic phase, as in Ref. [19]. At higher temperatures in the smectic *A* region the dipoles lay in the plane of the smectic layers and were orientationally degenerate. At lower temperatures the dipoles formed into ringlike domains and chains arranged so as to produce no overall spontaneous polarization. Similar results have been reported by Kachel and Gburski [21], and Berardi *et al.* [2] for transverse dipoles. A recent study by Berardi *et al.* [22] found ferroelectric nematic and smectic phases using a combination of a longitudinal steric dipole (''pear'' shape) and an off-center longitudinal electric dipole.

To date no studies have been reported where a dipolar potential has been included in the simulation of bent-core systems. In the study reported here we employ the a two-site Gay-Berne potential with a central transverse point dipole.

This paper is organised as follows: in Sec.II the model and details of the simulation are described, Sec. III contains the results and conclusions are presented in Sec. IV.

II. MODEL AND SIMULATIONS

A. Model

The bent-core molecular shape was modeled, as in the apolar study employing a two-site Gay-Berne [17]. The centres of mass were displaced by ± 0.5 reduced units to give an overall length-to-breadth ratio of 4:1 in the case of the rodlike, $\gamma=0°$, model, comparable to the real bent-core mesogens, e.g., P-*n*-PIMB [1]. The total potential is the sum of the Gay-Berne potential (V_{GB}) and the dipole-dipole interaction ($V_{\mu\mu}$),

$$V_{Total}=V_{GB}+V_{\mu\mu}. \tag{1}$$

The total potential energy is referred to as the polar Gay-Berne potential. The Gay-Berne potential is defined as

$$V_{GB}(\hat{\mathbf{u}}_i,\hat{\mathbf{u}}_j,\hat{\mathbf{r}}_{ij}) = 4\epsilon(\hat{\mathbf{u}}_i,\hat{\mathbf{u}}_j,\hat{\mathbf{r}}_{ij}) \times\left\{\left(\frac{\sigma_o}{(r_{ij}-\sigma(\hat{\mathbf{u}}_i,\hat{\mathbf{u}}_j,\hat{\mathbf{r}}_{ij})+\sigma_o)}\right)^{12} -\left(\frac{\sigma_o}{(r_{ij}-\sigma(\hat{\mathbf{u}}_i,\hat{\mathbf{u}}_j,\hat{\mathbf{r}}_{ij})+\sigma_o)}\right)^{6}\right\}, \quad (2)$$

where $\hat{\mathbf{u}}_i$ and $\hat{\mathbf{u}}_j$ are the orientational unit vectors and $\mathbf{r}_{ij}$ is the site-site intermolecular vector linking the centres of mass. The strength of the interaction is given by the strength anisotropy function, ϵ

$$\epsilon(\hat{\mathbf{u}}_i,\hat{\mathbf{u}}_j,\hat{\mathbf{r}}_{ij}) = \epsilon_o\epsilon_1^{\nu}(\hat{\mathbf{u}}_i,\hat{\mathbf{u}}_j)\epsilon_2^{\mu}(\hat{\mathbf{u}}_i,\hat{\mathbf{u}}_j,\hat{\mathbf{r}}_{ij}), \quad (3)$$

μ and ν are adjustable exponents and ϵ_o is a constant. ϵ_1 is defined by

$$\epsilon_1(\hat{\mathbf{u}}_i,\hat{\mathbf{u}}_j) = [1-\chi^2(\hat{\mathbf{u}}_i\cdot\hat{\mathbf{u}}_j)^2]^{-1/2}, \quad (4)$$

and ϵ_2 by

$$\epsilon_2(\hat{\mathbf{u}}_i,\hat{\mathbf{u}}_j,\hat{\mathbf{r}}_{ij}) = 1-\frac{\chi'^2}{2}\left(\frac{(\hat{\mathbf{r}}_{ij}\cdot\hat{\mathbf{u}}_i+\hat{\mathbf{r}}_{ij}\cdot\hat{\mathbf{u}}_j)^2}{1+\chi'\hat{\mathbf{u}}_i\cdot\hat{\mathbf{u}}_j} +\frac{(\hat{\mathbf{r}}_{ij}\cdot\hat{\mathbf{u}}_i-\hat{\mathbf{r}}_{ij}\cdot\hat{\mathbf{u}}_j)^2}{1-\chi'\hat{\mathbf{u}}_i\cdot\hat{\mathbf{u}}_j}\right), \quad (5)$$

χ' quantifies the anisotropy in the attractive forces and is defined in terms of the well depths, ϵ_s in the side-to-side configuration and ϵ_e in the end-to-end configuration.

$$\chi' = \frac{1-(\epsilon_e/\epsilon_s)^{1/\mu}}{1+(\epsilon_e/\epsilon_s)^{1/\mu}}. \quad (6)$$

Information about the shape of the molecule is then incorporated into the potential via the orientation-dependent range parameter

$$\sigma(\hat{\mathbf{u}}_i,\hat{\mathbf{u}}_j,\hat{\mathbf{r}}_{ij}) = \sigma_o\left[1-\frac{\chi}{2}\left(\frac{(\hat{\mathbf{r}}_{ij}\cdot\hat{\mathbf{u}}_i+\hat{\mathbf{r}}_{ij}\cdot\hat{\mathbf{u}}_j)^2}{1+\chi\hat{\mathbf{u}}_i\cdot\hat{\mathbf{u}}_j} +\frac{(\hat{\mathbf{r}}_{ij}\cdot\hat{\mathbf{u}}_i-\hat{\mathbf{r}}_{ij}\cdot\hat{\mathbf{u}}_j)^2}{1-\chi\hat{\mathbf{u}}_i\cdot\hat{\mathbf{u}}_j}\right)\right]^{-1/2}, \quad (7)$$

the parameter χ is defined by

$$\chi = \frac{(\sigma_e/\sigma_s)^2-1}{(\sigma_e/\sigma_s)^2+1}, \quad (8)$$

where σ_e/σ_s is the ratio of separations when the potential $V=0$, σ_e for the end-to-end configuration and σ_s for the side-to-side configuration. In this case $\sigma_0=\sigma_s$. Since its introduction, the Gay-Berne potential has been well characterized and successfully modeled a variety of liquid crystal phases e.g., Refs. [17,23–27]. The parameters used in the study here are the same as in Ref. [12], with $\sigma_e/\sigma_s=3$ and $\epsilon_e/\epsilon_s=0.2$ and μ and ν set to 2 and 1, respectively, to allow for comparison of the results obtained from the apolar bent-core study.

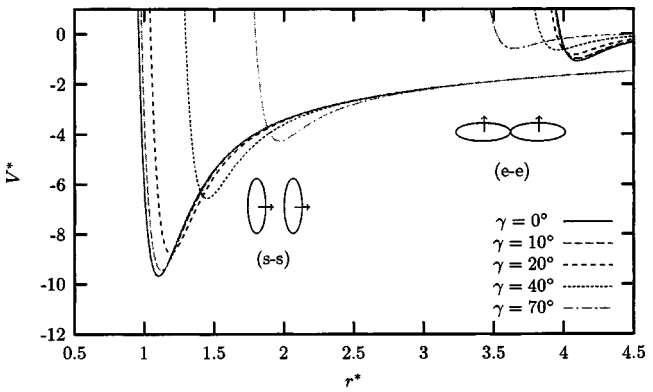

FIG. 2. The distance dependence of the potential energy calculated from the combined Gay-Berne and transverse dipole-dipole potential for side-to-side (s-s) and end-to-end (e-e) configurations of all models with respect to one another. The arrow represents the direction of the electric dipole.

The interaction potential due to a pair of dipoles is given below,

$$V_{\mu\mu} = \frac{\boldsymbol{\mu}_i\cdot\boldsymbol{\mu}_j - 3(\boldsymbol{\mu}_i\cdot\hat{\mathbf{r}}_{ij})(\boldsymbol{\mu}_j\cdot\hat{\mathbf{r}}_{ij})}{r_{ij}^3}, \quad (9)$$

where $\boldsymbol{\mu}_i=\mu\hat{\boldsymbol{\mu}}_i$, $\hat{\boldsymbol{\mu}}_i$ is the unit vector perpendicular to the molecular long axis, $\hat{\mathbf{u}}_i$, and μ is the magnitude of the dipole moment. The relevant axes are shown in Fig. 1(b). Long range correction to the dipole-dipole potential is accomplished in the present study by the reaction field method [28]. This method has been shown to be equivalent to the better known Ewald sum [29] method (see e.g. Refs. [30,31]) yet computationally more efficient. The reaction field method works by surrounding the particles inside the potential cut-off with a dielectric continuum. The pair interaction is given by

$$V_{\mu\mu} = V_{\mu\mu} - \frac{2(\epsilon_{RF}-1)}{2\epsilon_{RF}+1}\frac{\boldsymbol{\mu}_i\cdot\boldsymbol{\mu}_j}{r_c^3}, \quad (10)$$

where r_c is the potential cut-off distance. For $r_{ij}>r_c$, $V_{\mu\mu}$ is zero. A reduced dipole moment of $\mu^*=\mu^2/(4\pi\epsilon\epsilon_0\sigma_0^3)^{1/2}$ of 1.5 was employed in this study. The reaction field method has been used with ϵ_{RF} set to ∞ (tin-foil boundary conditions). This value was chosen because, like the real molecules, it provided the model with a strong transverse dipole moment of 2.27 D. This value was obtained by setting $\epsilon_0/k=302$ K and $\sigma_0=3\times10^{-10}$ m following Luckhurst *et al.* [27] in a study of mapping the Gay-Berne potential onto *p* terphenyl.

B. Simulations

The distance dependence of the potential energy calculated from the polar Gay-Berne potentials in the side-to-side

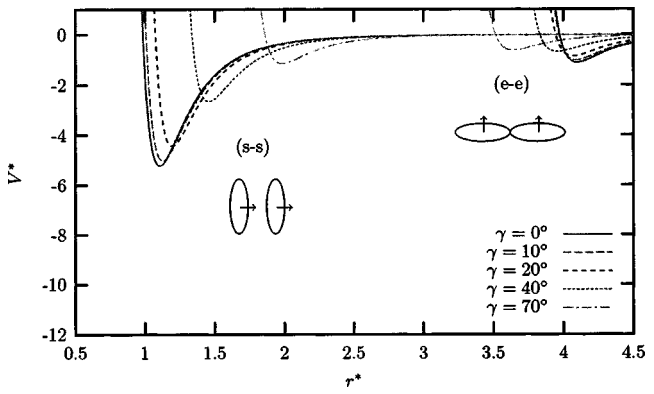

FIG. 3. The distance dependence of the potential energy calculated from the Gay-Berne potential for side-to-side (s-s) and end-to-end (e-e) configurations of all bent-core models with respect to one another. The arrow represents the direction of the steric dipole for $\gamma > 0°$.

and end-to-end configurations for all of the models studied with respect to one another is shown in Fig. 2. The minimum value of the potential energy can be seen to become less negative as the deviation is increased from the $\gamma = 0°$ case, presented for comparison, to $\gamma = 70°$ for the side-to-side configuration, shown in Fig. 2. As the value of γ is increased the intermolecular separation at which the minima in the potential energy occurs gradually increases. This is due to the ''wings'' of the bent-core shape preventing close alignment. If we compare the plots of the parallel interacting polar Gay-Berne models with those of the apolar models (Fig. 3) we see the potential energy has more negative minima in the polar case for the side-to-side configurations. This is due to the dipole acting transverse to the long molecular axis. We also see that the curve is steeper in the side-to-side configuration for all models indicating a ''harder'' total potential. No clear difference is seen in the end-to-end configuration between the polar and apolar models as expected because of the central position of the dipole. The effect of the dipole is more clearly seen in the potential energy contours for parallel interacting two-site Gay-Berne potentials with an additional central transverse electric dipole as a function of their separation, orientation and angle between the sites, shown in Figs. 4(a) to 4(e). We see the bent-core shape appearing at $\gamma = 10°$, Fig. 4(b). The bent-core shape is clearly visible in the $\gamma = 20°$ model shown in Fig. 4(c). This is further enhanced as the value of γ is increased from $\gamma = 20°$ [Fig. 4(c)] to $\gamma = 40°$, shown in Fig. 4(d). In the $\gamma = 40°$ model, we see that the length-to-breadth ratio has become less than in the rodlike case ($\gamma = 0°$) and in the final model, $\gamma = 70°$ [Fig. 4(e)] the bent-core shape has a much smaller length-to-breadth ratio than is commonly found in bent-core liquid crystal molecules. The addition of the dipole is evident in all the polar models with the enhancement of the potential energy contours perpendicular to the long molecular axis compared to the apolar model [12]. In the rodlike case ($\gamma = 0°$), this leads to a clearly noticeable ''waisted'' shape. The shifting of the pair potential minima (Fig. 2) for the end-to-end configuration is therefore explained by the consistent reduction of the length-to-breadth ratio as the value of γ increases.

The molecular dynamics simulation study reported here uses the same set of parameters as in a previous study of bent-core steric shape [12] to allow direct comparison. It was undertaken in the isothermal-isobaric ensemble (NPT) to best reflect realistic conditions and for systems of 1024 particles with periodic boundary conditions in a rectangular box with fixed aspect ratio of 1:1:2. The details of the isothermal-isobaric molecular dynamics simulations have been reported elsewhere [6,12,32]. Following Brown and Clarke [32] the pressure was calculated from the diagonal terms of the pressure tensor. For phases that appeared to be tilted the complete pressure tensor was calculated [33],

$$(P)_{\alpha\beta} = \frac{1}{V}\left[\sum_{i=1}^{N}\frac{1}{m}(p_i)_\alpha (p_i)_\beta + \sum_{i=1}^{N}\sum_{k=1}^{2}\sum_{j>i}^{N}\sum_{l=1}^{2}(F_{ij}^{kl})_\alpha (R_{ij}^{kl})_\beta\right], \tag{11}$$

where F_{ij}^{kl} is the force and R_{ij}^{kl} the separation between sites k and l on molecules i and j, respectively, p_i is the momentum of molecule i, m being the mass and V being the box volume. This enabled three diagonal components of the pressure tensor to be compared and the off-diagonal terms to be monitored checking for anisotropic stress.

All models were equilibrated in the isotropic phase and then cooled in steps of $T^*(\equiv kT/\epsilon_0) = 0.1$ or 0.2, the former used in close proximity of the systems to a phase transition. The pressure was kept constant at a value of P^* $(\equiv P\sigma^3/\epsilon_o)$ of 2.0 and the simulations were continued at each temperature until consecutive simulation runs produced identical results, within error. The final simulation run was then taken as the production run. Typical run lengths were between 400 000 and 600 000 steps. A reduced timestep of $\Delta t^* = 0.0005$ was used, reduced to $\Delta t^* = 0.000\,15$ when approaching a phase transition point, where $\Delta t^* \equiv \Delta t(m\sigma_0^2/\epsilon_o)^{1/2}$. All systems were cooled until a solid or near solid state was attained, determined from the second rank orientational order parameter Q_{00}^2.

The orientational order was analyzed using standard methods described in Refs. [34,35]. The tensor $\mathbf{Q^{xx}}$ used to measure orientational order is defined by

$$\mathbf{Q}_{\alpha\beta}^{\mathbf{xx}} = \frac{1}{N}\sum_{i=1}^{N}\frac{3\hat{x}_{i\alpha}\hat{x}_{i\beta} - \delta_{\alpha\beta}}{2}, \tag{12}$$

where $\hat{x}_i$ is a unit vector pointing along one axis of molecule i; $\mathbf{Q^{yy}}$ and $\mathbf{Q^{zz}}$ are defined similarly in terms of unit vectors $\hat{y}_i$ and $\hat{z}_i$ pointing along the other molecular axes. To obtain a system director, the dominant eigenvalue of each of $\mathbf{Q^{xx}}$, $\mathbf{Q^{yy}}$, and $\mathbf{Q^{zz}}$, was found, and the system director was identified with the eigenvector associated with the largest of these dominant eigenvalues; if necessary the molecule axes were relabeled so that this was an eigenvalue of $\mathbf{Q^{zz}}$. This

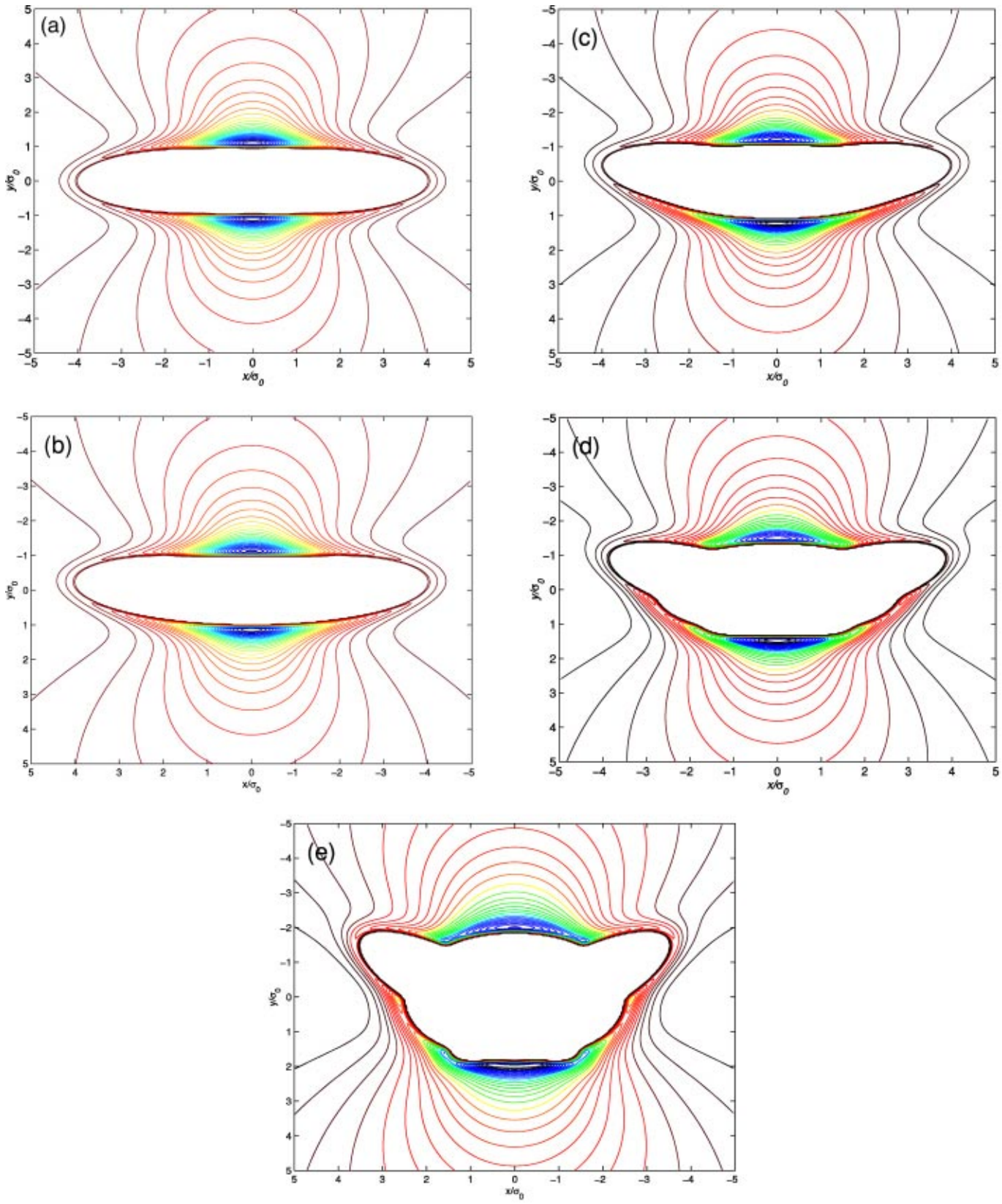

FIG. 4. Potential energy contours calculated for parallel molecules interacting via the Gay-Berne and transverse electric dipole potential as a function of their separation (coordinates of x and y are expressed in units of σ_0) and their orientation with respect to the intermolecular vector for (a) $\gamma=0°$, (b) $\gamma=10°$, (c) $\gamma=20°$, (d) $\gamma=40°$, and (e) $\gamma=70°$ in the xy plane.

direction defined the Z axis, $\hat{\mathbf{Z}}$. The order parameter Q_{00}^2 was then defined as $\langle \hat{\mathbf{Z}} \cdot \mathbf{Q}^{\mathbf{zz}} \cdot \hat{\mathbf{Z}} \rangle$, which coincides with the usual nematic order parameter $\langle P_2 \rangle$ calculated from experiment and simulation. To identify the Y axis, the largest dominant eigenvalue of $\mathbf{Q}^{\mathbf{xx}}$ and $\mathbf{Q}^{\mathbf{yy}}$ was considered, and the associated eigenvector taken; again, relabeling the molecule axes if necessary so that this direction is given by an eigenvector of $\mathbf{Q}^{\mathbf{yy}}$. As this direction was not, in general, orthogonal to the z axis, it was projected to the plane orthogonal to Z to give the Y axis, $\hat{\mathbf{Y}}$. Finally, the X axis was simply chosen to complete a right-handed system.

Biaxiality was measured by considering [34]

$$Q_{22}^2 = \frac{1}{3} \langle \hat{\mathbf{X}} \cdot \mathbf{Q}^{\mathbf{xx}} \cdot \hat{\mathbf{X}} + \hat{\mathbf{Y}} \cdot \mathbf{Q}^{\mathbf{yy}} \cdot \hat{\mathbf{Y}} - \hat{\mathbf{X}} \cdot \mathbf{Q}^{\mathbf{yy}} \cdot \hat{\mathbf{X}} - \hat{\mathbf{Y}} \cdot \mathbf{Q}^{\mathbf{xx}} \cdot \hat{\mathbf{Y}} \rangle. \tag{13}$$

This measures the extent to which the x and y molecular axes are ordered in the plane orthogonal to the system director, Z.

The layer normal in tilted systems was determined using simulated annealing [7,36]. Simulated annealing is particularly useful in situations where close minima occur. The method initially involves separating the system into n layers that will be analyzed to find the average layer normal $\hat{\mathbf{p}}$. This is accomplished by calculating the molecules projection onto the director and ''picking out'' layers, based on these values. Once the layers have been separated the best normal to the plane is obtained by minimizing the objective function χ shown below:

$$\chi^2 = \sum_j \sum_{i=1}^{m} (Ax_i + By_i + Cz_i - \langle d \rangle)^2, \tag{14}$$

where A, B and C are the directional cosines of the normal to the plane $\hat{\mathbf{p}}$. The longitudinal pair distribution function resolved parallel to the system normal, $g_{\parallel}(r_{\parallel}^*)_{\hat{\mathbf{p}}}$, can then be found via

$$g_{\parallel}(r_{\parallel}^*)_{\hat{\mathbf{p}}} = \frac{V}{N^2} \left\langle \sum_i \sum_{j \neq i} \delta |(\mathbf{r}^* - \mathbf{r}_{ij}^*) \cdot \hat{\mathbf{p}}| \right\rangle. \tag{15}$$

The angle of tilt, ϕ is then given by

$$\phi = \cos^{-1}(\hat{\mathbf{p}} \cdot \hat{\mathbf{Z}}). \tag{16}$$

To characterize the magnitude and sign of any chirality in the system following Xu *et al.* [10], the chiral order parameter

$$\langle \lambda \rangle = \frac{1}{N} \sum_{i=1}^{N} [(\hat{\mathbf{p}}_i \times \hat{\mathbf{u}}_i) \cdot \hat{\boldsymbol{\mu}}_i][\hat{\mathbf{p}}_i \cdot \hat{\mathbf{u}}_i] \tag{17}$$

was calculated. This order parameter is invariant under the symmetry operations $\hat{\mathbf{u}}_i \rightarrow -\hat{\mathbf{u}}_i$ and $\hat{\mathbf{p}}_i \rightarrow -\hat{\mathbf{p}}_i$ but not $\hat{\boldsymbol{\mu}}_i \rightarrow -\hat{\boldsymbol{\mu}}_i$.

The polar order $\langle P_1 \rangle$ is then given by

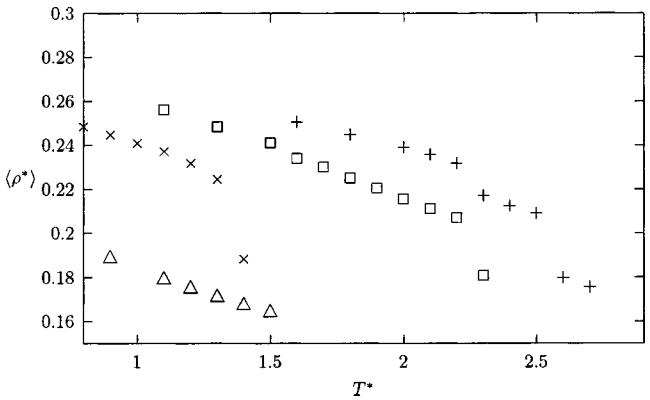

FIG. 5. Average scaled density, $\langle \rho^* \rangle$ as a function of scaled temperature T^* for the polar bent-core $\gamma = 10°$ (+), $\gamma = 20°$ (□), $\gamma = 40°$ (×), and $\gamma = 70°$ (△) models for $N = 1024$.

$$P_1 = \frac{1}{N} \sum_{i=1}^{N} \hat{\boldsymbol{\mu}}_i \cdot \hat{\mathbf{Y}}. \tag{18}$$

Structural information was obtained via the orientational averaged pair distribution function $g(r^*)$, the longitudinal $g_{\parallel}(r_{\parallel}^*)$, and transverse $g_{\perp}(r_{\perp}^*)$ pair distribution functions.

$$g(r^*) = \frac{V}{N^2} \left\langle \sum_i \sum_{j \neq i} \delta(\mathbf{r}^* - \mathbf{r}_{ij}^*) \right\rangle, \tag{19}$$

$$g_{\parallel}(r_{\parallel}^*)_{\hat{\mathbf{z}}} = \frac{V}{N^2} \left\langle \sum_i \sum_{j \neq i} \delta |(\mathbf{r}^* - \mathbf{r}_{ij}^*) \cdot \hat{\mathbf{Z}}| \right\rangle, \tag{20}$$

$$g_{\perp}(r_{\perp}^*)_{\hat{\mathbf{z}}} = \frac{V}{N^2} \left\langle \sum_i \sum_{j \neq i} \delta |(\mathbf{r}^* - \mathbf{r}_{ij}^*) \times \hat{\mathbf{Z}}| \right\rangle. \tag{21}$$

A spherical cutoff was used for $g(r^*)$ and a cylindrical volume was used in the calculation of $g_{\parallel}(r_{\parallel}^*)$ and $g_{\perp}(r_{\perp}^*)$, the axis of the cylinder being aligned along the director, Z. Further details of the simulation technique can be found in previous work [12].

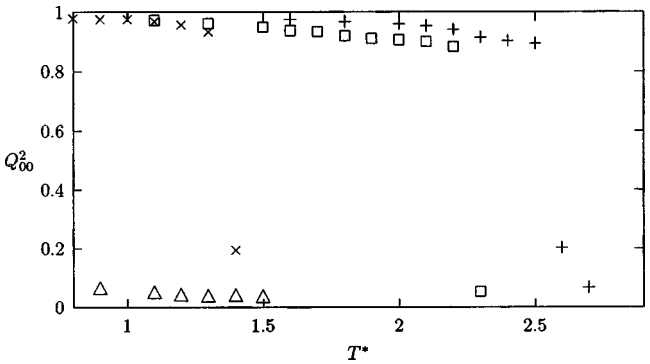

FIG. 6. Average second rank orientational order parameter Q_{00}^2 as a function of scaled temperature T^* for the polar bent-core $\gamma = 10°$ (+), $\gamma = 20°$ (□), $\gamma = 40°$ (×), and $\gamma = 70°$ (△) models for $N = 1024$.

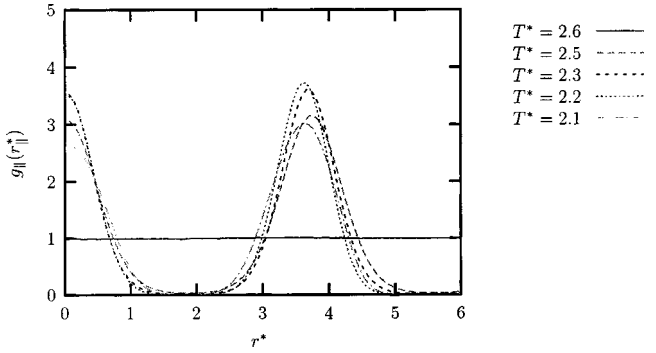

FIG. 7. Pair distribution functions for the polar $\gamma = 10°$ bent-core model resolved parallel to the director for a range of temperatures.

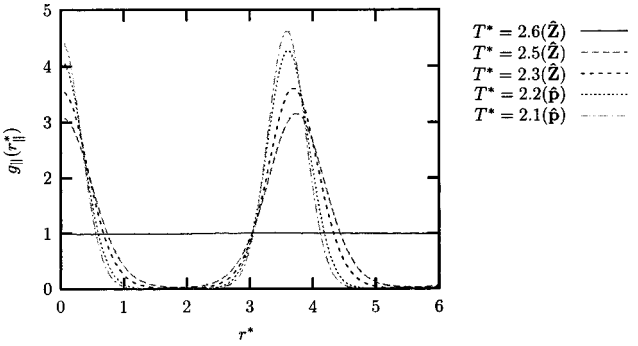

FIG. 9. Pair distribution functions for the polar $\gamma = 10°$ bent-core model resolved parallel to the director ($\hat{\mathbf{Z}}$) or layer normal ($\hat{\mathbf{p}}$) for a range of temperatures.

III. SIMULATION RESULTS AND DISCUSSION

Results are presented here for a series of polar bent-core models of varying angle between the sites.

A. $\gamma = 10°$ model

Figure 5 shows the variation in density as the systems were cooled and Fig. 6 shows the corresponding variation in the second rank orientational order parameter Q^2_{00} for $\gamma = 10°$, $\gamma = 20°$, $\gamma = 40°$, and $\gamma = 70°$.

Two phase transitions were seen to occur in the polar rodlike ($\gamma = 0°$) system [18]. At temperatures greater than $T^* = 2.6$, the system was seen to be fluid. As the temperature was reduced two phase transitions were seen, the first was to a smectic *B* phase, the second to a dense ferroelectric crystal. In comparison, the apolar system underwent a phase transition to nematic, smectic *A* and smectic *B* phases.

As the $\gamma = 10°$ system is cooled from the isotropic phase a discontinuity is seen in the density, Fig. 5, at a reduced temperature $T^* = 2.5$. For temperatures greater than $T^* = 2.5$, the value of the second rank orientational order parameter Q^2_{00} is not significant. No structure is seen in the radial and longitudinal pair distribution functions shown in Figs. 8 and 7, respectively.

At $T^* = 2.5$ the value of the second rank orientational order parameter increases to a value of 0.895 ± 0.005 from a value of 0.204 ± 0.033 at $T^* = 2.6$. An oscillation is seen in the longitudinal pair distribution function, $g_\parallel(r^*_\parallel)$, shown in Fig. 7, indicating a layered system. The first transition is between an isotropic liquid phase and a smectic *A* phase.

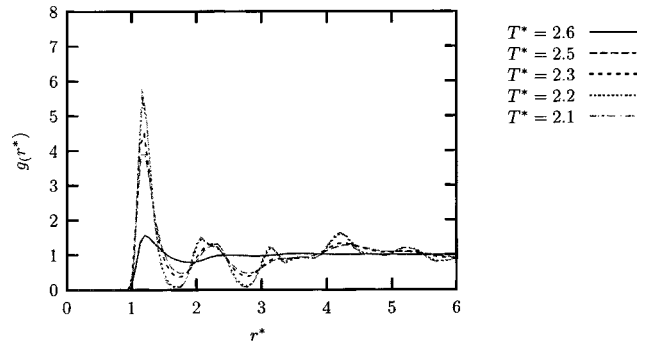

FIG. 8. Pair distribution functions for the polar $\gamma = 10°$ bent-core model for a range of temperatures.

Comparing the result for the first ordered phase of the steric only model [12], the polar $\gamma = 10°$ bent-core model has undergone the same first phase transition as the apolar model, from the isotropic phase to a smectic A phase. However, the temperature at which this occurs is higher for the polar bent-core model, $T^* = 2.5$, compared with $T^* = 2.3$ for the apolar bent-core model. Qualitatively there appears to be an enhancement of the layers in the polar bent-core model, detected by the greater magnitude of the oscillation and lesser width of the distribution, seen in the longitudinal pair distribution function, Fig. 7 compared with the apolar bent-core model [12].

As the temperature is reduced further a transition is seen to occur at $T^* = 2.2$, where an increase in the order parameter (Fig. 6) to 0.942 ± 0.004 from 0.914 ± 0.004 at $T^* = 2.3$ is accompanied by a discontinuity in the density (Fig. 5). Examination of the radial pair distribution function, $g(r^*)$ shown in Fig. 8, shows a split in the second peak between $r^* = 2.08$ and $r^* = 2.28$, indicate a hexagonal packing identifying this as a smectic *B* phase.

As the system is cooled further the maxima of the longitudinal pair distribution functions decrease in magnitude, shown in Fig. 7. This pattern of behavior is often seen in tilted systems where the tilting of the molecules smooths out the distribution function. To confirm whether or not the phase was tilted, a simulated annealing analysis was performed to determine whether a better plane normal than the system director could be found. The longitudinal pair distribution functions, resolved parallel to the layer normal, $g_\parallel(r^*_\parallel)_{\hat{\mathbf{p}}}$, after the simulated annealing analysis was performed, are shown in Fig. 9 for $T^* = 2.2$ and 2.1. After the simulated annealing a clear increase in the maxima of the oscillation in the longitudinal pair distribution function was seen (Fig. 9) for $T^* = 2.2$ and $T^* = 2.1$, confirming a better plane normal, $\hat{\mathbf{p}}$, than the system director $\hat{\mathbf{Z}}$ has been found, showing the presence of a tilted *B* phase. Above $T^* = 2.2$ no increase in the maxima of the oscillation was seen. Comparing this result with the apolar $\gamma = 10°$ bent-core model result [12] we see a subtle change. In the apolar case an increase in the layer spacing was detected as the system underwent a phase transition to a smectic *B* phase from a smectic *A* phase.

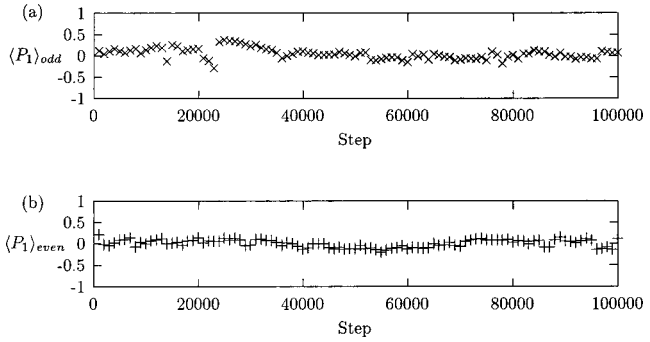

FIG. 10. Average electric polar order parameter $\langle P_1\rangle$ from a set of adjacent (a) odd and (b) even layers for the polar $\gamma=10°$ model, calculated every 1000 simulation steps for $N=150$ at $T^*=2.1$.

However, no tilting of the molecules or unusual in-plane order was found. With the addition of a transverse electric dipole the transition has been from a smectic *A* phase to a tilted smectic *B* phase. A potential problem of the fixed aspect ratio box is that it may affect equilibrium layer formation. However, this would be indicated by an off axis component in the pressure tensor and unequal diagonal components. This is not present in any of the studies undertaken here.

To determine whether there was any odd or even structure, the layers were separated and analyses performed separately. This was accomplished as follows; for each step, *j* in the simulation the first layer with more than 50 molecules, termed the ''even layer'' and the adjacent ''odd'' layer were identified. 150 molecules from each layer were then used to calculate the polar order parameter for the layer from

$$\langle P_1\rangle_{even}=\frac{1}{150n_{\text{steps}}}\sum_{i=1}^{n_{\text{steps}}}\sum_{\substack{\text{even layers}\\ j=1}}^{150}\hat{\boldsymbol{\mu}}_j\cdot\hat{\mathbf{Y}}, \tag{22}$$

$$\langle P_1\rangle_{odd}=\frac{1}{150n_{\text{steps}}}\sum_{i=1}^{n_{\text{steps}}}\sum_{\substack{\text{odd layers}\\ j=1}}^{150}\hat{\boldsymbol{\mu}}_j\cdot\hat{\mathbf{Y}}, \tag{23}$$

TABLE I. Results for the electric polar order parameter $\langle P_1\rangle$ and angle of tilt for the $N=1024$ simulations in the *NPT* ensemble for the polar $\gamma=10°$ bent-core model.

T^*	$\langle P_1\rangle$	Tilt (deg)
2.7	0.000(0.024)	
2.6	0.009(0.025)	
2.5	0.015(0.031)	
2.4	0.015(0.039)	
2.3	−0.014(0.041)	
2.2	0.021(0.061)	6.20(1.11)
2.1	0.004(0.047)	7.78(0.09)
2.0	0.005(0.058)	9.46(0.24)
1.8	−0.019(0.117)	8.64(0.91)
1.6	0.036(0.154)	7.98(0.03)
1.5	−0.437(0.550)	7.61(1.16)

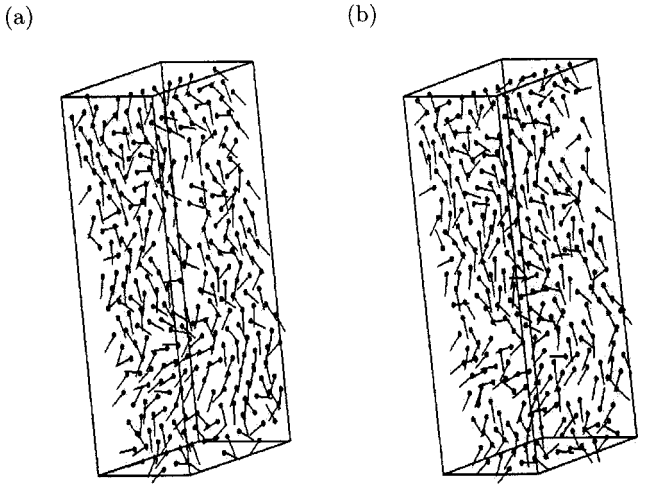

FIG. 11. A snapshot of a section of layers from the production run at $T^*=1.5$ for the polar $\gamma=10°$ bent-core model for adjacent (a) odd and (b) even layers. The centers of mass are represented by the spheres, the line vector, −, indicates the polar axis of the molecule.

where n_{steps} is the total number of steps in the production run. The analysis of the polar order parameter, $\langle P_1\rangle$ is shown in Fig. 10 for $T^*=2.1$. No significant value of $\langle P_1\rangle$, $\langle P_1\rangle_{even}$ or $\langle P_1\rangle_{odd}$ was found in the smectic *B* phase despite the addition of a transverse electric dipole. Comparison of the results of the simulated annealing for the separated odd and even layers shows the direction of tilt is the same in adjacent layers indicating the phase is synclinic in tilt. Hence the effect of a combination of steric and electric transverse dipole has been shown, in this case, to result in the production of a tilted smectic *B* phase. These tilted phases persist down to the lowest temperature studied, $T^*=1.5$, with a tilt angle in the range $6.2°\pm1.1°$ to $9.5°\pm0.2°$. The results of the tilt analysis are shown in Table I.

As the temperature is reduced further to $T^*=1.5$ the system is seen to develop an overall value for the polar order parameter $\langle P_1\rangle=-0.4\pm0.5$ shown in Table I indicating the phase has some overall polarization which changes in direction during the simulation. A snapshot of two adjacent layers and the results of the odd or even analysis are shown in Figs.

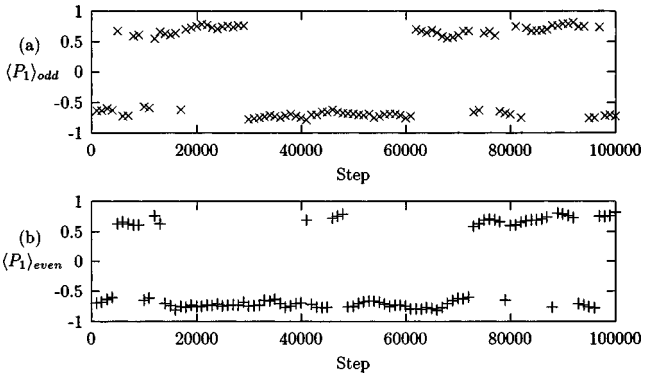

FIG. 12. Average electric polar order parameter $\langle P_1\rangle$ from a set of adjacent (a) odd and (b) even layers for the polar $\gamma=10°$ model, calculated every 1000 simulation steps for $N=150$ at $T^*=1.5$.

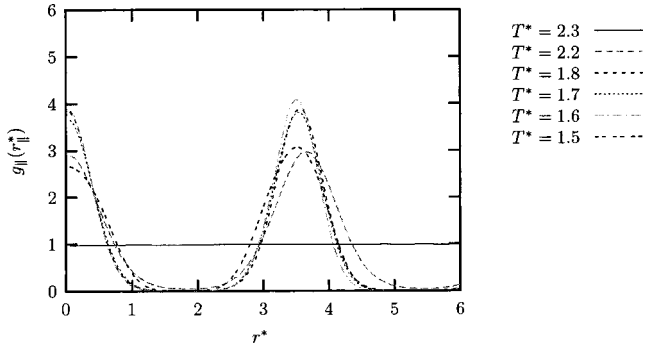

FIG. 13. Pair distribution functions for the polar $\gamma = 20°$ bent-core model resolved parallel to the director for a range of temperatures.

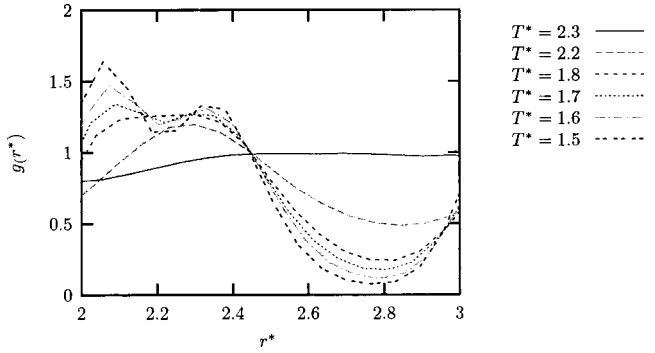

FIG. 14. Radial pair distribution functions for the polar $\gamma = 20°$ bent-core model for a range of temperatures. Radial pair distribution functions displayed in the region of $r^* = 2.0$ to $r^* = 3.0$ for the polar $\gamma = 20°$ bent-core model for a range of temperatures.

11 and 12, respectively. From Fig. 11 the overall polarization of adjacent layers can be seen to be in the same direction and this is confirmed by the values of $\langle P_1 \rangle_{odd}$ and $\langle P_1 \rangle_{even}$ calculated for adjacent layers (Fig. 12). The polarization oscillates between approximately ± 0.6, however, adjacent layers tend to align in the same direction at the same step, i.e. swapping the overall direction of polarization together. This is attributed to the low value of γ allowing free rotation about the long molecular axis, and therefore the direction of polarization to change. In contrast, a spontaneously polarized crystal was seen for the polar rodlike model [18]. Here the polarized phase is seen in a tilted smectic B phase. The bent-core has had the effect of allowing the development of a spontaneous polarization whilst remaining fluid albeit in a dense smectic phase. This model has therefore reproduced the tilted ferroelectric phase of the $B2$ phase, however, no hexagonal ordering is seen in the real $B2$ molecular systems.

B. $\gamma = 20°$ model

As the $\gamma = 20°$ system is cooled from the isotropic phase, a discontinuity is seen in the density at $T^* = 2.2$, shown in Fig. 5. For temperatures greater than this the value of Q^2_{00} is less than 0.051 ± 0.019, as we would expect for an isotropic system. Furthermore, no structure is seen in the pair distribution functions. The first transition is identified by a discontinuity in the density at $T^* = 2.2$, as shown in Fig. 5, and an increase in the second rank orientational order parameter Q^2_{00} (Fig. 6) which increases from 0.051 ± 0.019 at $T^* = 2.3$ to 0.881 ± 0.005 at $T^* = 2.2$. An oscillation occurs at this temperature in the longitudinal pair distribution function $g_{\parallel}(r^*_{\parallel})$ shown in Fig. 13. The radial pair distribution function $g(r^*)$ remains liquidlike showing this to be a smectic A phase.

Comparing the simulation of the apolar $\gamma = 20°$ model [12] and the polar $\gamma = 20°$ bent-core model presented here, we see an increase in the temperature of transition from the isotropic to the first ordered phase from $T^* = 2.0$ to $T^* = 2.2$, respectively. Furthermore we see the first transition has changed from between the isotropic and nematic phase for the apolar $\gamma = 20°$ model to between the isotropic and smectic A phase for the polar $\gamma = 20°$ model [12].

A second transition is seen for the polar bent-core $\gamma = 20°$ model at $T^* = 1.7$. No clear discontinuity is visible in the density, Fig. 5, however, the second rank orientational order parameter Q^2_{00} increases from 0.918 ± 0.004 at $T^* = 1.8$ to 0.931 ± 0.003 at $T^* = 1.7$. The longitudinal pair distribution function $g_{\parallel}(r^*_{\parallel})$ (Fig. 13) has a slight reduction in the amplitude of its oscillation indicating a disruption of the layers with respect to the higher temperature $T^* = 1.8$. Over the range $T^* = 1.7$ to $T^* = 1.5$, the radial pair distribution function $g(r^*)$ develops a split in the second peak showing a change in the in-plane structure from liquidlike to hexagonal. This is more clearly seen in Fig. 14 which shows only the region around the second peak in the radial pair distribution function. This region is identified as a tilted smectic region, however, it is not clearly hexagonal but some hexagonal character may be appearing as pretransitional order with a small discontinuity occurring in the density between $T^* = 1.6$ and $T^* = 1.5$. Examination of the longitudinal pair distribution functions shown in Fig. 13 reveals a trend seen previously in the apolar $\gamma = 20°$ bent-core model [12] and in the polar $\gamma = 10°$ bent-core model described earlier in this report. As the temperature is reduced, the amplitude of $g_{\parallel}(r^*_{\parallel})$ is decreasing in magnitude. These results were analyzed using the simulated annealing technique to see whether any difference existed between the director and the layer

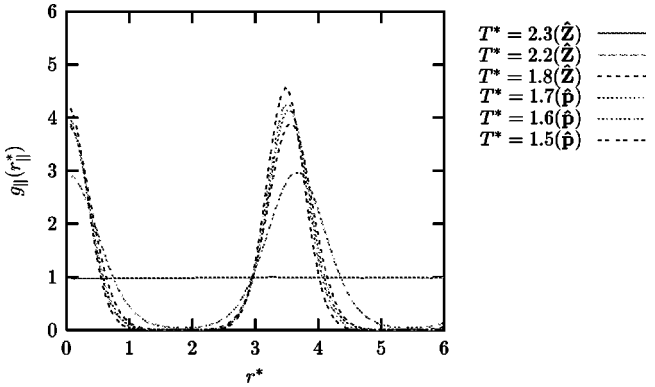

FIG. 15. Pair distribution functions for the polar $\gamma = 20°$ bent-core model resolved parallel to the director ($\hat{\mathbf{Z}}$) or layer normal ($\hat{\mathbf{p}}$) for a range of temperatures.

TABLE II. Results for the electric polar order parameter $\langle P_1 \rangle$ and angle of tilt for the $N=1024$ simulations in the NPT ensemble for the polar $\gamma=20°$ bent-core model.

T^*	$\langle P_1 \rangle$	Tilt (deg)
2.3	−0.010(0.018)	
2.2	0.001(0.033)	
2.1	−0.014(0.040)	
2.0	−0.008(0.041)	
1.9	−0.012(0.060)	
1.8	0.054(0.053)	
1.7	−0.013(0.044)	4.1(1.1)
1.6	0.014(0.044)	7.2(3.2)
1.5	−0.032(0.020)	8.1(2.2)
1.3	−0.038(0.024)	10.4(0.9)
1.1	−0.097(0.013)	14.5(1.0)

normal. The results of the analyses are shown in Fig. 15. We can see that for temperatures $T^*=1.7$ to $T^*=1.5$ the peaks have become better defined and have increased in magnitude. The angles of tilt, $\phi=\cos^{-1}(\hat{\mathbf{p}}\cdot\hat{\mathbf{Z}})$, are presented in Table II. The phases in the region $T^*=1.7$ to $T^*=1.1$ are identified as tilted smectic B phases with angles increasing from 4.1° ±1.1° at $T^*=1.7$ to 14.5°±1.0° at $T^*=1.1$. We have already seen that the addition of a transverse electric dipole can lead to a tilted phase when combined with a transverse steric dipole for $\gamma=10°$. Here we see that the the addition of a transverse electric dipole has led to a greater maximum tilt angle compared with the apolar case [12] where tilt angles of 3.3°±0.9° and 12.5°±5.7° were found for $\gamma=20°$. In both cases the angles of tilt is less than that found in real bent-core phases of approximately 25° to 35°, e.g., Refs. [37,15]. A snapshot of the tilted phase at $T^*=1.2$ is shown below in Fig. 16.

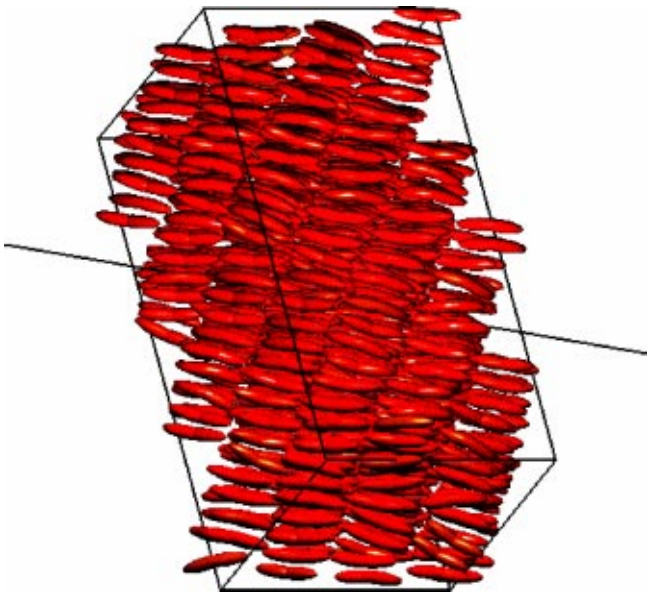

FIG. 16. A snapshot from the production run of the polar $\gamma=20°$ bent-core model at $T^*=1.2$.

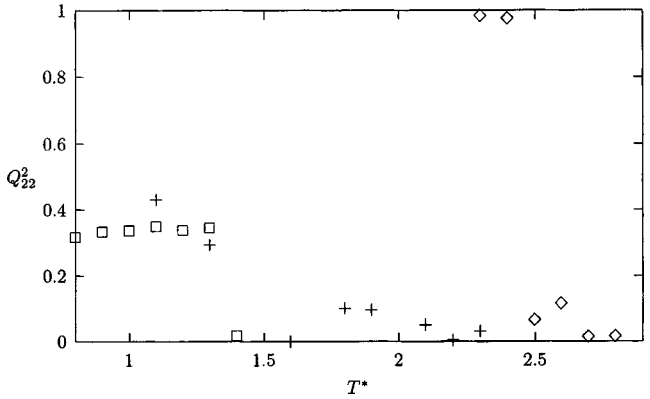

FIG. 17. Average biaxial order parameter Q_{22}^2 as a function of scaled temperature T^* for the rod (◇) and bent-core $\gamma=20°$ (+) and $\gamma=40°$ (□) models for $N=1024$.

Examination of the values for the Q_{22}^2 biaxiality parameter show an increase as the temperature is reduced to $T^*=1.3$, from -0.010 ± 0.060 at $T^*=1.5$ to 0.294 ± 0.038 at $T^*=1.3$ illustrated in Fig. 17. For temperatures above $T^*=1.3$ the values of Q_{22}^2 are nonsignificant. Interestingly there is no sign of a ''TGB-like'' phase [12] formed by the steric model where a difference in the minor eigenvalues was apparent due to the formation of 'striped' regions with different local directors. In this case, for the polar $\gamma=20°$ model, the difference in the minor eigenvalues is very small. Here the biaxiality is due to the alignment of the subsidiary molecular axes in the plane orthogonal to the director. As such this can be considered a uniform biaxial phase.

To determine whether any odd or even layer effect existed the layers were separated and analyses performed on the separated layers at $T^*=1.5$ and below, as before. For systems with temperatures above $T^*=1.5$ the layers were found to be too disordered to be analyzed using this method. The separation of the layers often failed to provide any representative sample of particles in subsequent layers for further analysis. In the tilted smectic B phase the aim was to determine whether any antiparallel packing existed. Parallel packing was already excluded due to the nonsignificant $\langle P_1 \rangle$ calculated for the whole system (Table II). The results of the $\langle P_1 \rangle$ analysis for the separated layers of the polar $\gamma=20°$

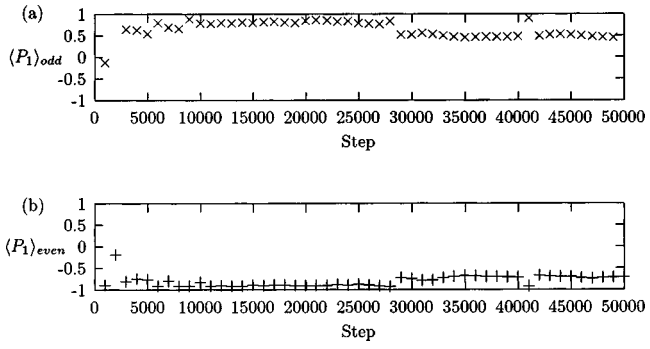

FIG. 18. Average electric polar order parameter $\langle P_1 \rangle$ from a set of adjacent (a) odd and (b) even layers for the polar $\gamma=20°$ model, calculated every 1000 simulation steps for $N=150$ at $T^*=1.3$.

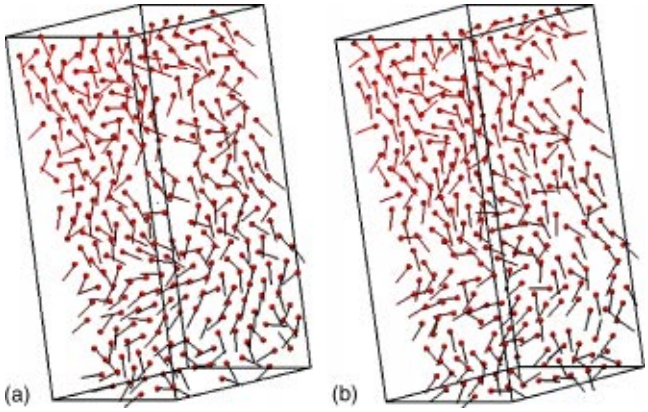

FIG. 19. A snapshot of a section of layers from the production run at $T^*=1.3$ for the polar $\gamma=20°$ bent-core model for adjacent (a) odd and (b) even layers. The centers of mass are represented by the spheres, the line vector, $-$, indicates the polar axis of the molecule.

model at $T^*=1.3$ are shown in Fig. 18 and is typical of all temperatures between $T^*=1.5$ and $T^*=1.1$ for this model. It is clearly seen that adjacent layers have values of $\langle P_1\rangle$, $\langle P_1\rangle_{odd}$, and $\langle P_1\rangle_{even}$ that are opposite in sign but approximately the same magnitude. This results in an average $\langle P_1\rangle$ for the system that is nonsignificant, although each layer is polarized. The value of $\langle P_1\rangle$ in adjacent layers is approximately ± 0.6 indicating a strong polarization. A snapshot of sections of two adjacent layers is shown in Fig. 19. This polarization was not seen for the apolar case where $\langle P_1\rangle$, $\langle P_1\rangle_{odd}$, and $\langle P_1\rangle_{even}$ were all zero. Thus for the temperature region $T^*=1.5$ to $T^*=1.1$ the phase was identified as an antiferroelectric tilted smectic B phase. A further simulated annealing analysis was performed on the separated layers to determine whether the system was anticlinic or synclinic. Adjacent layers were found to be tilted in the same direction indicating that the phase was synclinic. This is

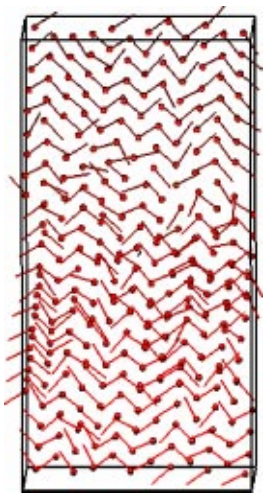

FIG. 20. A snapshot of a section of a layer from the production run at $T^*=0.8$ for the polar $\gamma=40°$ bent-core model. The centers of mass are represented by the spheres, the black lines vector, $-$, indicates the direction of the polar axis of the molecule.

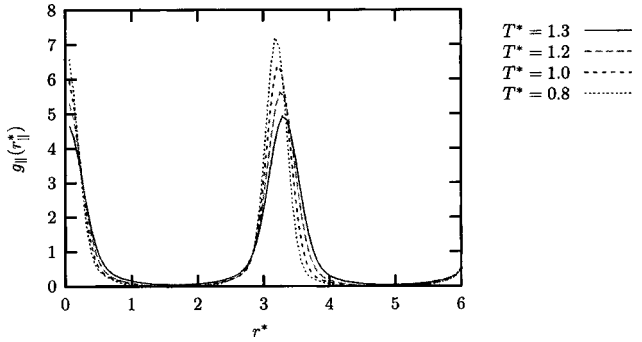

FIG. 21. Pair distribution functions for the polar $\gamma=40°$ bent-core model resolved parallel to the director for a range of temperatures.

close in phase structure to a phase of real bent-core molecules, however, the bent-core smectic hexagonal B-type phase, the $B3$ phase, is not tilted. This type of synclinic antiferroelectric phase is one of those predicted by Brand *et al.* [13] to be chiral. Further cooling does not produce any further phase transitions.

This phase may be considered to be racemic and not chiral following the Boulder model [38]. This is confirmed by the chiral order parameter $\langle\lambda\rangle$ that has a value of 0.12 ± 0.13 and is not significant.

C. $\gamma=40°$ model

As the system was cooled, a transition occurred at a temperature of $T^*=1.3$. This transition can be seen from the discontinuity in the density shown in Fig. 5 and the increase in the orientational order parameter, Q^2_{00} (Fig. 6), to 0.933 ± 0.003 at $T^*=1.3$ from 0.194 ± 0.019 at $T^*=1.4$. Again we see the first transition occurring at a higher temperature for the polar model compared with the apolar $\gamma=40°$ model [12] which occurred at $T^*=1.0$. Similarly to the apolar case [12] we see the temperature of transition is lower for the $\gamma=40°$ bent-core model than for the rodlike, $\gamma=10°$ and $\gamma=20°$ models. The longitudinal pair distribution function $g_\parallel(r^*_\parallel)$shown in Fig. 21 displays an oscillation indicating the presence of a layered system. The large maximum value and narrow width of the oscillations in $g_\parallel(r^*_\parallel)$ indicate a well ordered layered structure. The radial pair distribution func-

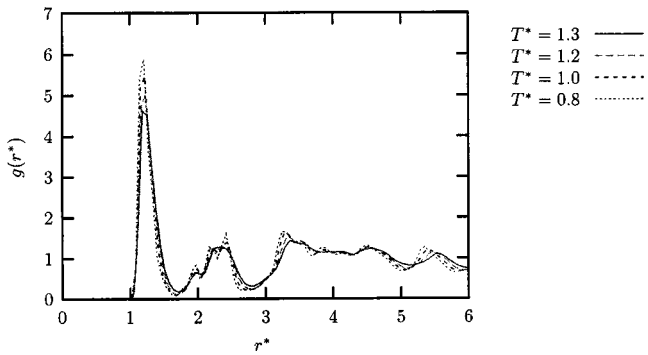

FIG. 22. Pair distribution functions for the polar $\gamma=40°$ bent-core model for a range of temperatures.

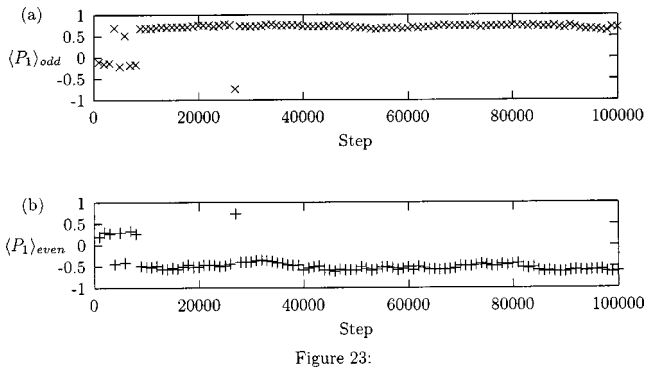

FIG. 23. Average electric polar order parameter $\langle P_1 \rangle$ from a set of adjacent (a) odd and (b) even layers for the polar $\gamma = 40°$ bent-core model, calculated every 1000 simulation steps for $N = 150$ at $T^* = 0.8$.

tion $g(r^*)$ shown in Fig. 22 displays an unusual pattern. The main peaks appear to have associated with them smaller peaks, particularly, a small peak at $r^* = 2.0$. A peak at this position was found in the apolar $\gamma = 40°$ bent-core model [12] and is attributed to the existence of in-plane T configurations since the overall length-to-breadth ratio of the model is approximately 3:1. This was confirmed by visual inspection. A snapshot of the phase at $T^* = 0.8$ is shown in Fig. 20 where *T* shaped arrangement of the dipoles is apparent. The different configurations possible for a bent-core system are; back-to-back, face-to-face, and back-to-face, as well as a wide range of T and X configurations. There is no clear split of the second peak that would indicate the formation of hexagonal packing. A split is seen to be developing in the complex set of peaks at $r^* = 2.0$, 2.1, and 2.4 indicating a mix of configurations. This transition is therefore between the isotropic phase and a smectic *X* phase which does not fall into the usual classification. The addition of the transverse electric dipole has led to a change in the first ordered phase of the $\gamma = 40°$ bent-core model. The apolar $\gamma = 40°$ model underwent a first transition to a ''TGB-like phase'' [12]. With the addition of an electric dipole this first transition has changed to a smectic *X* phase. This complexity of packing is seen in the real liquid crystal bent-core mesogens where there remains considerable discussion on the identification of phases of real molecules.

Examination of the biaxial order parameter Q_{22}^2 shown in Fig. 17 reveals the system has self-organised into a biaxial phase. Unlike the apolar $\gamma = 40°$ bent-core model, the polar model has not formed into a ''TGB-like'' biaxial phase but has formed a uniform biaxial smectic *X* phase where the subsidiary axes are ordered in the plane perpendicular to the system director. The effect of the transverse electric dipole on this model has been to maintain long-range orientation of the smectic layers which were disrupted by the purely steric shape. The biaxiality parameter remains significant as the temperature is decreased confirming its stability.

The same odd or even analysis was performed on the polar $\gamma = 40°$ model that was conducted for the previous models. The results of the analyses are shown in Fig. 23 from the production run at $T^* = 0.8$. As was found earlier for the polar $\gamma = 20°$ model, the effect of the dipole on the system has been to produce high degrees of spontaneous polarization within a layer that is, on average, canceled by the next layer, hence, $\langle P_1 \rangle$ is zero. The value of $\langle P_1 \rangle_{odd/even}$ was found to be, approximately ± 0.5, the sign alternating between layers. This phase thus is classified as an antiferroelectric smectic *X* phase. Unlike the polar $\gamma = 20°$ bent-core model studied, the polar $\gamma = 40°$ model does not have any in-layer tilt of the molecules; confirmed using the simulated annealing analysis hence is racemic. This model has reproduced the main features of a real bent-core phase, the $B3$ phase in Pelzl's description [16]. The simulated phase is a nontilted smectic phase, has polar ordering of the molecular axes with some disorder still present, however, hexagonal order is not dominant. No further phase transitions are seen as the system is cooled.

D. $\gamma = 70°$ model

It has already been commented on that this model is closest to the real bent-core molecules in terms of its value of γ, however, its length-to-breadth ratio is unrealistic. No transitions are evident from examination of the variation in density, ρ^* and second rank orientational order parameter Q_{00}^2 shown in Figs. 5 and 6, respectively. Reduction in the reduced temperature T^* results in an increase in the density as expected but the value of Q_{00}^2 never attains a significant value. Examination of the pair distribution function $g(r^*)$ and the longitudinal pair distribution function $g_{\|}(r_{\|}^*)$reveal no structure at any temperature.

This behavior was also seen in the apolar $\gamma = 70°$ bent-core model [12]. The length-to-breadth ratio is no longer a realistic approximation to that of a real bent-core molecule. The static value of the second rank orientational order parameter Q_{00}^2at a value of 0.060 ± 0.006 indicates that, as was found for the apolar case, the particles have formed interlocking pairs and frozen into a plastic state.

IV. CONCLUSIONS

We have undertaken a series of simulations of polar bent-core molecules. We employed a simple model of the bent-core molecules comprising a two site Gay-Berne potential with a central transverse dipole and we varied the angle γ between the sites from 10° to 70°. The addition of the transverse electric dipole to the potential was seen to affect the temperature range and type of phase formed with a trend towards ordered phases at higher temperatures compared to the steric only model. The link between larger steric dipole and lower temperatures of onset of the first ordered phase remained.

The polar $\gamma = 10°$ and $\gamma = 20°$ bent-core models underwent two phase transitions, the first was to a smectic *A* phase and the second to a tilted smectic *B* phase. The effect of the electric dipole on the polar $\gamma = 10°$ model was to enhance the layer structure of the smectic *A* phase compared with that of the apolar $\gamma = 10°$ bent-core model. The addition of a transverse electrical dipole on the $\gamma = 20°$ model was found to destabilise the nematic phase compared to the apolar model

with the first transition between the isotropic and a smectic *A* phase. The tilted smectic *B* phases of the polar $\gamma=10°$ and $\gamma=20°$ bent-core models were found to have a synclinic tilt of the molecules with respect to the layer normal reproducing some of the behavior of the real molecules. They were racemic and not chiral. However, in real bent-core molecules the in-plane hexagonal ordering, whilst being present in the *B*3 bent-core phase, is not seen in conjunction with molecular tilt. Upon further cooling of the smectic *B* phase of the polar $\gamma=10°$ bent-core model the system developed polar ordering. This was found to alternate in direction, but adjacent layers were, on average aligned in the same direction. On examination of adjacent layers for the polar $\gamma=20°$ model in the smectic *B* phase, high spontaneous polarization within each layer was found but adjacent layers spontaneously ordered to give an antiferroelectric structure with no overall $\langle P_1 \rangle$.

The polar $\gamma=40°$ model underwent a first transition to a homeotropic biaxial smectic *X* phase and a second transition to an antiferroelectric biaxial smectic *X* phase. This is compared with the apolar $\gamma=40°$ model which underwent a first phase transition to a ''TGB-like phase'' and then showed no further phase transitions. The transverse electric dipole has again had the effect of reinstating the long-range ordering of the smectic layers that are disrupted by the purely steric bent-core shape. Hence the steric and electric dipole are having contrary effects on the packing for this magnitude of electric dipole. In both the polar and apolar systems the packing was complex with a range of orientations indicated by the broad second peak in the pair distribution function. Some of these features have been attributed to T configurations of the dipoles within the layer.

In the case of apolar bent-core models tilting of the molecules within the layer was found only at $\gamma=20°$. With the addition of the transverse electric dipole to the transverse steric dipole shape, the structure of the phases changed. The polar $\gamma=10°$ model formed a tilted phase and the polar $\gamma=20°$ bent-core model attained higher degrees of tilt than in the case of the apolar model. This leads to the conclusion that a transverse electric dipole in conjunction with a transverse steric dipole shape can lead to tilted phases, although within a range of $0^o<\gamma<40°$ for the models studied. For a sufficiently biaxial shape, $20^o<\gamma<70°$, the addition of the electric dipole leads to the development of antiferroelectric biaxial structures in the lowest temperature phases.

The polar bent-core models have been successful in simulating many of the complex features of real bent-core molecules. They have highlighted the stabilization of the smectic phase and increased tilt shown with the addition of the transverse electric dipole. The link between delayed onset of ordered phases and larger steric dipole, was enhanced by the addition of the electric dipole.

ACKNOWLEDGMENTS

The authors would like to thank the Engineering and Physical Sciences Research Council which has funded this work, Grant No. GR/L76693. One of the authors, S.J., is grateful to the EPSRC for providing financial support. The authors would like to acknowledge useful conversations with Dr. Martin Grayson of Sheffield University.

[1] T. Niori, T. Sekine, J. Watanabe, T. Furukawe, and H. Takezoe, J. Mater. Chem. **6**, 1231 (1996).
[2] R. Berardi, S. Orlandi, and C. Zannoni, Int. J. Mod. Phys. C **10**, 477 (1999).
[3] E. Gwozdz and A. Brodka, Acta. Phys. Pol. A **98**, 645 (2000).
[4] S. McGrother, A. Gil-Villegas, and G. Jackson, Mol. Phys. **95**, 657 (1998).
[5] A.G. Petrov and A. Derzhanski, Mol. Cryst. Liq. Cryst. **89**, 339 (1987).
[6] M.P. Neal, A.J. Parker, and C.M. Care, Mol. Phys. **91**, 603 (1997).
[7] M.P. Neal and A.J. Parker, Mol. Cryst. Liq. Cryst. **330**, 565 (1999).
[8] P.J. Camp, M.P. Allen, and A.J. Masters, J. Chem. Phys. **74**, 3316 (1999).
[9] R. Memmer and G. Schobel, Liq. Cryst. **29**, 483 (2000).
[10] J. Xu, R.L.B. Selinger, J.V. Selinger, and R. Shashidar, J. Chem. Phys. **115**, 4333 (2001).
[11] P.K. Maiti, Y. Lansac, M.A. Glaser and N.A. Clark, Phys. Rev. Lett. **88**, 65504 (2002).
[12] S.J. Johnston, R.J. Low, and M.P. Neal, Phys. Rev. E **65**, 050706 (2002).
[13] H.R. Brand, P.E. Cladis, and H. Pleiner, Eur. Phys. J. B **6**, 347 (1998).
[14] D.E. Link, G. Natale, R. Shao, J.E. Maclennan, N.A. Clark, D.M. Körblova, and D.M. Walba, Science **278** (1997).
[15] S. Diele, S. Grande, H. Kruth, C.H. Lischka, G. Pelzl, W. Weissflog, and I. Wirth, Ferroelectrics **212**, 169 (1998).
[16] G. Pelzl, S. Diele, and W. Weissflog, Adv. Mater. **11**, 707 (1999).
[17] J.G. Gay and B.J. Berne, J. Chem. Phys. **74**, 3316 (1981).
[18] S. J. Johnston, R. J. Low, and M. P. Neal, Ferroelectrics (to be published).
[19] M. Houssa, A. Oualid, and L.F. Rull, Mol. Phys. **94**, 439 (1998).
[20] A. Gil-Villegas, S.C. McGrother, and G. Jackson, Chem. Phys. Lett. **269**, 441 (1997).
[21] A. Kachel and Z. Gburski, J. Phys.: Condens. Matter **9**, 1095 (1997).
[22] R. Berardi, M. Ricci, and C. Zannoni, Chem. Phys. **2**, 443 (2001).
[23] G.R. Luckhurst, R.A. Stephens, and R.W. Phippen, Liq. Cryst. **8**, 451 (1990).
[24] M.A. Bates and G.R. Luckhurst, J. Chem. Phys. **110**, 7087 (1999).
[25] R. Berardi, A.P.J. Emerson, and C. Zannoni, J. Chem. Soc., Faraday Trans. **89**, 4069 (1993).
[26] E. de Miguel, L.F. Rull, M.K. Chalam, and K.E. Gubbins, Mol. Phys. **74**, 405 (1991).
[27] G.R. Luckhurst and P.J. Simmonds, Mol. Phys. **80**, 233 (1993).

[28] J.A. Barker and R.O. Watts, Mol. Phys. **26**, 789 (1973).
[29] P. Ewald, Ann. Phys. (San Diego) **64**, 253 (1921).
[30] M. Houssa, L.F. Rull, and S.C. McGrother, J. Chem. Phys. **109**, 9529 (1998).
[31] C.G. Gray, Y.S. Sainger, C.G. Joslin, P.T. Cummings, and S. Goldman, J. Chem. Phys. **85**, 1502 (1986).
[32] D. Brown and J.H.R. Clarke, Mol. Phys. **51**, 1243 (1984).
[33] S. Nose and M.L. Klein, Mol. Phys. **50**, 1055 (1983).
[34] M.P. Allen, Liq. Cryst. **8**, 499 (1990).
[35] C. Zannoni, *The Molecular Physics of Liquid Crystals*, Computer Simulation (Academic Press, London, 1979).
[36] W. H. Press, S. A. Teukolsky, W. T. Vetterling, and B. P. Flannery, *Numerical Recipes in Fortran, 2nd ed*. (Cambridge University Press, Cambridge, 1986).
[37] J.P. Bedel, J.C. Rouillon, J.P. Marcerou, M. Laguerre, M.F. Achard, and H.T. Nguyen, Liq. Cryst. **27**, 103 (2000).
[38] D.E. Link, G. Natale, R. Shao, J.E. Maclennan, N.A. Clark, E. Körblova, and D.M. Walba, Science **278**, 1924 (1997).